

Smectic Aggregates of Sheet-Like Side-Chain Liquid Crystalline Polyacetylenes Directly Formed During Solution Polymerization

Lu-Mei Liu,[†] Kai-Peng Liu,[†] Yu-Ping Dong,[‡] Er-Qiang Chen,^{*,†} and Ben Zhong Tang^{*,§}

[†]Beijing National Laboratory for Molecular Sciences, Department of Polymer Science and Engineering and the Key Laboratory of Polymer Chemistry and Physics of Ministry of Education, College of Chemistry and Molecular Engineering, Peking University, Beijing 100871, China, [‡]College of Material Science and Engineering, Beijing Institute of Technology, Beijing 100871, China, and [§]Department of Chemistry, The Hong Kong University of Science & Technology, Clear Water Bay, Kowloon, Hong Kong, China

Received March 22, 2010; Revised Manuscript Received June 7, 2010

ABSTRACT: We have successfully synthesized two side-chain liquid crystalline polyacetylenes (denoted as P3-5 and P2-5) with the mesogenic units based on a “phenyl–ester–phenyl” motif directly linked to the semirigid polyacetylene backbone in a terminal-on mode *without* flexible spacer. During the polymerization catalyzed by Rh(nbd)[B(C₆H₅)₄] in toluene, the resultant polymers (or oligomers) automatically precipitate out of the polymerization solution as red solids, which cannot be dissolved in common organic solvents. Wide-angle X-ray diffraction results confirm that the polymer precipitates possess a smectic (or sanidic) structure, suggesting that the molecules *without* flexible spacers are sheet-like and can stack parallel to each other during polymerization. We in situ monitored the solution polymerization and the aggregation processes using UV–visible and ¹H NMR spectroscopy methods. The experimental results indicate that after reaching a critical molecular weight the P3-5 and P2-5 molecules self-aggregate in solution and that the smectic aggregation proceeds during the solution polymerization. An apparent first-order polymerization kinetics can be obtained after the polymerization and aggregation slowed down. The resultant polymers are *cis*-rich with the main-chain absorption at ~455 nm. This implies that a considerably long effective conjugation length is achieved in the sheet-like *cis*-rich polyacetylene derivatives.

Introduction

In the past few decades many researchers have endeavored to develop liquid crystalline (LC) polyacetylenes.^{1–6} From a viewpoint of technological applications, introducing side-chains with mesogenic moieties to the conjugated polyacetylene main-chain may result in new types of functional polymers which combine the different molecular electronic and optical properties.⁶ In general, the synthetic strategy of side-chain LC polyacetylenes (SCLCPAs) also follows the concept of “flexible spacer”,⁷ which is widely used in the synthesis of conventional side-chain LC polymers with flexible main-chains. To effectively decouple the dynamics of the fairly rigid polyacetylene main-chain and the mesogenic side-chains, flexible spacer with a reasonably long length in SCLCPA plays an important role in the LC phase formation. Le Moigne et al. have reported for the first time a SCLCPA with the bulky cholesteryl mesogenic group placed at the end of the flexible spacers.⁸ Another early example is a group of side-chain LC poly(1-pentyne)s synthesized by Akagi and Shirakawa, in which the polyene main-chain and the phenylcyclohexyl unit are bridged through an ether functional group.^{9,10} After those early works, many studies on the subject of SCLCPAs have been published.^{11–14} A body of experimental results have confirmed that the flexible spacer is crucial with respect to the LC behaviors of SCLCPAs, particularly considering that the rigid polyacetylene backbone might somewhat hinder the LC phase formation.³ For example, Tang et al. have systematically studied the LC properties of SCLCPAs with different flexible spacer length.^{15,16} They have found that an increase in the spacer length

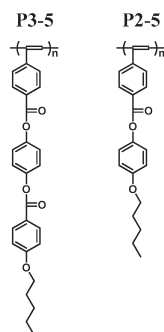
of poly(*n*-{[(4'-heptoxy-4-biphenyl)oxy]carbonyl}-1-alkyne)s can cause the LC phase to change from mixed mono- and bilayer smectic structures to a homogeneous monolayer smectic structure.¹⁵ For a series of poly(*n*-{[(4'-cyano-4-biphenyl)oxy]carbonyl}-1-alkyne)s, while the polymer with a spacer of two methylene units just forms a nematic phase, increasing the number of the methylene units to 8 results in smectic phase.¹⁶ Therefore, one may conclude that the longer the flexible spacer is, the better the mesogenic order the SCLCPA will have. In this context, the LC phases of SCLCPAs are largely dependent on the LC properties of the mesogenic groups on the side-chains, but the contribution of conjugated backbone to LC phase formation has been paid little attention.

However, the polyacetylene backbone itself in fact can be part of the building block of the LC phase structure, considering its semirigid and anisotropic nature. It is well-known that the main-chain rigid rods bearing aromatic backbones can display nematic phase.¹⁷ When flexible side-chains are introduced to the rigid rod, two limiting conformations of the individual chain molecules can be envisioned.¹⁸ If the side-chains wrap the rigid backbone in a more or less uniform manner, the chain molecule is cylindrical and can pack into columnar LC phases. On the other hand, if the side-chains and the backbone share approximately a same plane, the molecular shape looks sheet- or board-like. According to Wendorff et al., the board-like chain molecules can form various sanidic LC phases.¹⁸ In both the limiting cases, the rigid backbone dominates the shape persistency, which is essential to the LC phase formation. In this regard, we believe that further evaluating the role of the polyacetylene backbone playing in LC phases is worth doing.

Here, we still focus on SCLCPAs containing typical rod-like mesogenic moieties. Of particular interest is to ask: when the

*To whom correspondence should be addressed. E-mail: (E.-Q.C.) eqchen@pku.edu.cn; (B.Z.T.) tangbenz@ust.hk.

Chart 1. Chemical Structures of P3-5 and P2-5

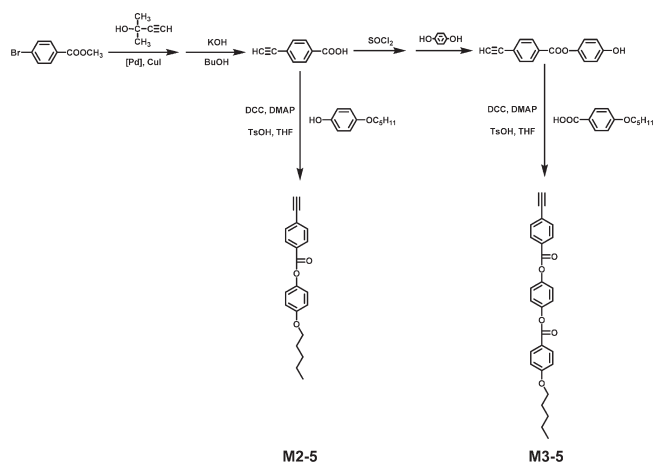


spacer is gradually shortened until its absence, or in other words, when the dynamics of the polyacetylene backbone and mesogenic side groups becomes hard to be decoupled, what will the LC phase behavior and the molecular shape of the SCLCPA be? Costa et al. have investigated the influence of short spacer on the phase formation of SCLCPA.^{19–21} They have found that the polymers with only a short flexible spacer may exhibit enantiotropic smectic phase behavior, even though the monomers do not show any LC properties. Moreover, the polymers with a three methylene spacer exhibit a double layer tilted smectic structure, while those with only a single methylene inserted between the backbone and mesogens can have an interdigitated smectic structure. According to these results, it is very possible that the LC phases are constructed by the backbone and side-chains in a cooperative manner. Recently, we have reported that a *trans*-rich poly(5-[[4'-heptoxy-4-biphenyl]carbonyl]oxy}-1-pentyne) with the spacer containing three methylene units exhibits a highly ordered smectic phase with a frustrated structure of molecular packing.²² The building block of the LC phase is actually the whole chain molecule with a sheet-like (or ribbon-like) shape, of which the side-chains are parallel but extend to opposite directions on both sides of the backbone. Furthermore, we have found that the sheet-like molecules can self-assemble into monolayer lamellae in dilute solutions with the solvents selective for the side-chain tails.²³ In this case, the backbone and mesogens are tightly coupled together, which shall be attributed to the rather short spacer of three methylene units.

So far the results published in literatures suggest that the side-chain polyacetylene with the mesogenic moieties terminally attached to the backbone *without* flexible spacer cannot render any LC structure.^{24–27} However, from a simple geometric point of view, it is still possible that directly linking the rod- or lath-like mesogenic groups to the polyacetylene backbone with highly regular stereostructure (either *cis* or *trans*) can result in a planar structure,^{24,25} giving sheet-like polyacetylene derivatives which can pack parallel to form smectic LC structure or sanidic structure.¹⁸ Such sheet-like polyacetylene molecule is of interest, because the unique molecular architecture may lead to a greatly improved effective conjugation, and thus may offer better electronic and optical properties for the polyacetylenes amenable for advanced applications.^{10,28}

In this paper, we intend to construct sheet-like polyacetylenes with high shape persistency by directly attaching the mesogenic units to the semirigid backbone in a terminal-on mode *without* flexible spacer. Two poly(phenylacetylene) (PPA) derivatives (denoted as P3-5 and P2-5) were synthesized and characterized carefully, whose chemical structures are shown in Chart 1. Without any spacer, the portion of “backbone + mesogenic cores” shall be rather rigid if the main-chain stereoregularity is adequately high. We found that the solution polymerization using Rh(nbd)-[B(C₆H₅)₄] (nbd = 2,5-norbornadiene) catalyst directly afforded bright red polymer aggregates with smectic (or sanidic) structure.

Scheme 1. Synthetic Routes to the Monomers M2-5 and M3-5



Our wide-angle-X-ray diffraction (WAXD) data indicate that the sheet-like molecules can be considered as the building block of smectic (or sanidic) structure. Similar to that observed in other systems,²⁹ the aggregation during polymerization resulted in quite uniform nanosized polymer particles. On the basis of in situ monitoring of the polymerization processes by UV–vis and ¹H NMR techniques, which have been seldom used in kinetic study of acetylene polymerization,³⁰ we found that the ordered packing of smectic structure occurred just after the polymer molecules had reached a “critical molecular weight”. The *cis*-rich polymers showed a main-chain absorption at ~455 nm, indicative of a considerably long effective conjugation length. Furthermore, an apparent first-order polymerization kinetics was observed after the polymerization and aggregation had slowed down during the solution polymerization process.

Experimental Section

Materials. 2-Methyl-3-butyn-2-ol (Alfa Aesar), bis(triphenylphosphine)palladium(II) chloride (Acros), copper(I) iodide (Acros), 4-dimethylamino-pyridine (Acros), (bicyclo[2.2.1]hepta-2,5-diene)chlororhodium(I) dimer ([Rh(nbd)Cl]₂, Aldrich), and 2,5-norbornadiene (Alfa Aesar) were all purchased and used without further purification. The solvents were treated as follows: tetrahydrofuran (THF), triethylamine (Et₃N), and toluene were dried over calcium hydride, potassium hydroxide, and sodium under nitrogen, respectively. Other chemicals were obtained from Beijing Chemical Co. and were used as received.

Synthesis of Monomers. The synthetic route to the monomers M3-5 and M2-5 is shown in Scheme 1.

(a). *Synthesis of 4-Ethynylbenzoic Acid.* The reaction procedures are similar to that reported elsewhere.³¹ To a 250 mL three-necked flask were added methyl 4-bromobenzoate (25 g, 116 mmol), 2-methyl-3-butyn-2-ol (15 mL, 154 mmol), Ph₃P (0.3 g, 1.15 mmol), CuI (87 mg, 0.46 mmol) in 100 mL of dry Et₃N and 40 mL of dry pyridine. PdCl₂(Ph₃P)₂ (80 mg, 0.12 mmol) was then added to the above mixture under nitrogen. After refluxing for 2.5 h at ca. 88 °C, the mixture was cooled to room temperature and was filtered to remove the insoluble triethylamine hydrobromide. The salt was washed with triethylamine and ethyl ether until the ether washings were clear. The combined filtrates were reduced to dryness under reduced pressure, and the crude product was washed with water. The residue was dried under vacuum to yield 22 g of methyl 4-(3-hydroxy-3-methylbut-1-ynyl) benzoate. The above solid was dissolved in 300 mL of refluxing solution of *n*-butanol with 25 g of KOH. After refluxing for 10 min, the mixture was cooled in an ice-bath. After filtration, the collected residue was acidified to pH 2 by HCl. The mixture was extracted with ethyl acetate. After removing the solvent, the residue was dried under vacuum to

yield 12 g of 4-ethynylbenzoic acid as yellow solids (yield 82%). ^1H NMR (400 MHz, CDCl_3), δ (ppm): 8.07 (d, 2H, Ar-H ortho to COOH), 7.59 (d, 2H, Ar-H meta to COOH), 3.27 (s, 1H, $\equiv\text{CH}$).

(b). *Synthesis of 4-[(4-Hydroxyphenyl)oxycarbonyl]phenylacetylene*. Potassium 4-ethynylbenzoate (2 g) was added to dry THF with two drops of dimethylformamide (DMF). The mixture was cooled with an ice bath, to which 2 mL of SOCl_2 was added dropwise. The mixture was then refluxed for 1.5 h. Afterward, the solution was concentrated by a rotary evaporator to give an orange solid of 4-ethynylbenzoyl chloride. Hydroquinone (2.5 g) was dissolved in dry THF with a small amount of pyridine, to which a THF solution of 4-ethynylbenzoyl chloride was added under stirring via a dropping funnel with a pressure-equalization arm. The reaction mixture was refluxed for 8 h and then the solvent was removed by a rotary evaporator. The crude product was purified by column chromatography using petroleum ether/ethyl acetate (3/1, v/v) as the eluent. After recrystallization from ethanol, 4-[(4-hydroxyphenyl)oxycarbonyl]phenylacetylene was obtained as white solids (1.9 g, yield 65%). ^1H NMR (400 MHz, CDCl_3), δ (ppm): 8.17–8.14 (d, 2H, Ar-H ortho to COO), 7.64–7.61 (d, 2H, Ar-H ortho to $\text{C}\equiv\text{CH}$), 7.09–7.06 (d, 2H, Ar-H ortho to OOC), 6.88–6.85 (d, 2H, Ar-H ortho to OH), 4.85 (s, 1H, OH), 3.28 (s, 1H, $\equiv\text{CH}$).

(c). *Synthesis of 4-(Pentyloxy)benzoic Acid*. 4-Hydroxybenzoic acid (14 g, 0.1 mol) and KI (0.1 g) were dissolved in 50 mL of ethanol, to which 12 g (0.21 mol) of KOH in 10 mL of water was added dropwise with stirring. After being cooled, the reaction mixture was titrated dropwise with 0.1 mol of 1-bromopentane. After refluxing for 24 h, the reaction mixture was poured into a large amount of water, followed by acidification to pH 3–4 by HCl. The white precipitate was filtered, washed with water and recrystallized in ethanol. 4-(Pentyloxy)benzoic acid was obtained as white solids. ^1H NMR (400 MHz, CDCl_3), δ (ppm): 12.62 (s, 1H, COOH), 7.90–7.86 (d, 2H, Ar-H ortho to COOH), 7.04–7.00 (d, 2H, Ar-H ortho to OCH_2), 4.05–4.03 (t, 2H, OCH_2), 1.85–1.81 (m, 2H, OCH_2CH_2), 1.47–1.41 (m, 4H, $\text{CH}_2\text{CH}_2\text{CH}_3$), 0.97–0.93 (t, 3H, CH_3).

(d). *Synthesis of 4-(Pentyloxy)phenol*. The compound was prepared according to the literature method with some modification.³² Hydroquinone (11 g, 0.1 mol) was dissolved in 100 mL of dimethyl sulfoxide (DMSO), to which 16.8 g (0.3 mol) of powdered KOH was added under stirring. Within 0.5 h, 0.1 mol of 1-bromopentane was added to the above mixture under stirring via a dropping funnel with a pressure-equalization arm. The reaction mixture was kept in 40 °C water bath with vigorous stirring for 3 h and the course of reaction was followed by TLC. When completed, the reaction mixture was poured into 400 mL cold water followed by acidification to pH 1. The crude product was filtered out and washed with cold water. After purified by column chromatography using dichloromethane (DCM) as the eluent, 4-(pentyloxy)phenol was obtained as white solid in a yield of ca. 20%. ^1H NMR (400 MHz, CDCl_3), δ (ppm): 6.80–6.73 (m, 4H, Ar-H), 4.53 (s, 1H, OH), 3.90 (t, 2H, OCH_2), 1.76 (m, 2H, OCH_2CH_2), 1.43–1.36 (m, 4H, $\text{CH}_2\text{CH}_2\text{CH}_3$), 0.92 (t, 3H, CH_3).

(e). *Synthesis of 4-[4-(Pentyloxy)benzoyloxy]phenyl 4-Ethynylbenzoate (M3-5)*. First, 0.5 g (2.1 mmol) of 4-[(4-hydroxyphenyl)oxycarbonyl]phenylacetylene, 1.0 g (4.8 mmol) of 4-(pentyloxy)benzoic acid, 0.15 g (1.3 mmol) of DMAP, 0.23 g (1.2 mmol) of TsOH were dissolved in 100 mL of dry DCM, to which the DCM solution of 1.5 g (7.3 mmol) of DCC was added dropwise with stirring. The reaction mixture was stirred for 24 h at room temperature. After the solvent was removed, the crude product was purified by a silica gel column using petroleum ether/DCM (1:1 by volume) as eluent. M3-5 was obtained as white solid in a yield of ca. 60%.

^1H NMR (400 MHz, CDCl_3), δ (ppm): 8.18–8.13 (t, 4H, Ar-H meta to $\text{C}\equiv\text{CH}$ or OCH_2), 7.64–7.61 (d, 2H, Ar-H ortho to $\text{C}\equiv\text{CH}$), 7.26 (s, 4H, Ar-H ortho to OOC), 6.99–6.97 (d, 2H, Ar-H ortho to OCH_2), 4.07–4.03 (t, 2H, OCH_2), 3.28 (s,

1H, $\equiv\text{CH}$), 1.85–1.82 (m, 2H, OCH_2CH_2), 1.47–1.40 (m, 4H, $\text{CH}_2\text{CH}_2\text{CH}_3$), 0.97–0.94 (t, 3H, CH_3). ^{13}C NMR (100 MHz, CDCl_3), δ (ppm): 164.79, 164.38 (COO), 163.63 (aromatic carbon linked with OC_5H_{11}), 148.67, 148.12 (aromatic carbon linked with OOC), 132.30 (aromatic carbon ortho to $\text{HC}\equiv\text{C}$), 132.27 (aromatic carbon ortho to COO and meta to OC_5H_{11}), 130.05 (aromatic carbon linked with COO and para to $\text{HC}\equiv\text{C}$), 129.40 (aromatic carbon ortho to COO and meta to $\text{HC}\equiv\text{C}$), 127.54 (aromatic carbon linked with $\text{HC}\equiv\text{C}$), 122.77, 122.47 (aromatic carbon ortho to OOC), 121.35 (aromatic carbon linked with COO and para to OC_5H_{11}), 114.34 (aromatic carbon ortho to OC_5H_{11}), 82.68 ($\text{HC}\equiv\text{C}-$), 80.57 ($\text{HC}\equiv\text{C}-$), 68.34 (OCH_2), 28.79 ($\text{OCH}_2\text{CH}_2\text{CH}_2\text{CH}_2\text{CH}_3$), 28.13 ($\text{OCH}_2\text{CH}_2\text{CH}_2\text{CH}_2\text{CH}_3$), 22.42 ($\text{OCH}_2\text{CH}_2\text{CH}_2\text{CH}_2\text{CH}_3$), 13.99 (CH_3). MS: $m/z = 428$ (M^+). Anal. Calcd for $\text{C}_{27}\text{H}_{24}\text{O}_5$: C, 75.68; H, 5.65; Found: C, 75.43; H, 5.64.

(f). *Synthesis of 4-(Pentyloxy)phenyl 4-Ethynylbenzoate (M2-5)*. Monomer M2-5 was synthesized by esterification of 4-ethynylbenzoic acid with 4-(pentyloxy)phenol. The experimental procedures were similar to those for the synthesis of M3-5 described above. Monomer M2-5 was obtained as white solid in a yield of 60%.

^1H NMR (400 MHz, CDCl_3), δ (ppm): 8.15 (d, 2H, Ar-H meta to $\text{C}\equiv\text{CH}$), 7.61 (d, 2H, Ar-H ortho to $\text{C}\equiv\text{CH}$), 7.10 (d, 2H, Ar-H meta to OCH_2), 6.93 (d, 2H, Ar-H ortho to OCH_2), 3.96 (t, 2H, OCH_2), 3.27 (s, $\equiv\text{CH}$), 1.79 (m, 2H, OCH_2CH_2), 1.47–1.38 (m, 4H, $\text{CH}_2\text{CH}_2\text{CH}_3$), 0.94 (t, 3H, CH_3). ^{13}C NMR (100 MHz, CDCl_3), δ (ppm): 164.79 (COO), 157 (aromatic carbon linked with OC_5H_{11}), 144.13 (aromatic carbon para to OC_5H_{11}), 132.17 (aromatic carbon ortho to $\text{C}\equiv\text{CH}$), 129.94 (aromatic carbon meta to $\text{C}\equiv\text{CH}$), 129.70 (aromatic carbon para to $\text{C}\equiv\text{CH}$), 127.32 (aromatic carbon linked with $\text{C}\equiv\text{CH}$), 122.25 (aromatic carbon meta to $\text{OC}_{12}\text{H}_{25}$), 115.13 (aromatic carbon ortho to $\text{OC}_{12}\text{H}_{25}$), 82.72 ($\text{HC}\equiv\text{C}-$), 80.41 ($\text{HC}\equiv\text{C}-$), 68.43 (OCH_2), 29.67 (OCH_2CH_2), 29.08 ($\text{CH}_2\text{CH}_2\text{CH}_3$), 22.42 (CH_2CH_3), 13.97 (CH_3). MS: $m/z = 308$ (M^+). Anal. Calcd for $\text{C}_{20}\text{H}_{20}\text{O}_3$: C, 77.92; H, 6.49; Found: C, 77.96; H, 6.33.

(g). *Synthesis of Rh(nbd)[B(C₆H₅)₄] Catalyst*. Synthesis of this catalyst was carried out according to the method reported by Schrock et al.³³ $\text{RhCl}_3 \cdot 3\text{H}_2\text{O}$ (250 mg) was dissolved in water (1 mL), and $\text{Na}[\text{B}(\text{C}_6\text{H}_5)_4]$ (1 g) in methanol (20 mL) was added. 2,5-Norbornadiene (nbd; 1 mL) was then added and the solution was allowed to stand until crystals were deposited. The yellow crystalline products were filtered and air-dried. The desired complex was obtained in a yield of ca. 70%. Anal. Calcd for $\text{C}_31\text{H}_{28}\text{RhB}$: C, 72.40; H, 5.49; Found: C, 70.14; H, 5.41.

Polymerization. Using $\text{Rh}(\text{nbd})[\text{B}(\text{C}_6\text{H}_5)_4]$ as catalyst and dry toluene as solvent, a typical procedure for the polymerization of M3-5 is as follows: Into a polymerization tube was added 7×10^{-3} mmol (3 mg) of monomer M3-5, and then 3 mL of dry toluene with 0.2 mg of $\text{Rh}(\text{nbd})[\text{B}(\text{C}_6\text{H}_5)_4]$ was put into the tube. After 24 h reaction at room temperature, the red suspension of polymer product was directly filtered out. After being washed three times with acetone, the product was dried under vacuum to a constant weight. The yield was over 80%.

Instruments and Measurements. Elemental analysis was performed with an Elementar Vario EL instrument. Mass spectra were recorded on a Finnigan-MAT ZAB-HS spectrometer. FT-IR and Raman measurements were carried out using a Magna-IR750 (Nicolet) FT-IR spectrometer and an IFS-106 (Bruker) Raman spectrometer, respectively. Differential scanning calorimetry (DSC, PerkinElmer Pyris I with a mechanical refrigerator) was utilized to study the phase transitions of the monomers and the polymers. Thermogravimetric analysis (TGA) was performed with a TA SDT 2960 instrument at a heating rate of 10 °C/min in nitrogen or air atmosphere. Gel permeation chromatography (GPC) was carried out on a Waters 515 GPC instrument using THF as an eluent at 35 °C. The GPC calibration curve was obtained with linear polystyrene standards.

UV–vis absorption and turbidity measurements were performed with a Lambda 35 (Perkin-Elmer) UV–vis spectrometer.

We followed the change of UV–vis absorption during polymerization. The polymerization was carried out in a 1 cm colorimetric container in open air at room temperature. The absorption from 350 to 750 nm was recorded continuously right after adding $\text{Rh}(\text{nbd})[\text{B}(\text{C}_6\text{H}_5)_4]$ to the toluene solution. The turbidity was measured at a wavelength of 700 nm, and the solvent of dry toluene was used as the reference.

^1H NMR (400 MHz) spectra were recorded on a Bruker ARX400 spectrometer at room temperature using deuterated chloroform (CDCl_3) as the solvent and tetramethylsilane (TMS) as the internal standard. To monitor the polymerization process by ^1H NMR, the in situ measurement was carried out on a Mercury Plus (Varian) 300 MHz spectrometer. In an NMR tube, M3-5 was dissolved in toluene- d_6 (~ 10 mg/mL) with trace of DCM as an internal standard. The spectra were recorded sequentially immediately after the addition of $\text{Rh}(\text{nbd})[\text{B}(\text{C}_6\text{H}_5)_4]$.

To identify the LC structure of the polymer particles, WAXD experiments were performed with a high-flux small-angle X-ray scattering instrument (SAXSess, Anton Paar) equipped with Kratky block-collimation system and a Philips PW3830 sealed-tube X-ray generator ($\text{Cu K}\alpha$). The diffraction patterns were recorded on an imaging-plate which extends to the high-angle range (up to 2θ of 42°). The diffraction peak positions were calibrated with silver behenate.

After the polymerizations completed, the morphology of polymer particles was examined using scanning electron microscopy (SEM; JEOL JSM-6700F). The SEM sample was prepared by placing a drop of the polymerization suspension on a clear silica surface with the excess solution blotted by a filter paper. After drying under ambient conditions and later in vacuum, the SEM sample was sputtered with a gold layer.

Computer Modeling. Single molecules of P3-5 and P2-5 containing 10 repeating units with a perfect *cis*-transoidal structure of the polyacetylene backbone were constructed by Materials Studio 5.0 (Accelrys). We further assumed that the alkyl tails on side chains were in all *trans* conformation. The energy of this molecule was minimized using Smart Minimizer incorporated in the Discover Molecular Simulation Program.

Results and Discussion

We attempted to investigate the molecular shape and LC properties of polyacetylene derivatives with the mesogenic units directly linked to the polyacetylene backbones without flexible spacer. In order to easily tune the length and thus the aspect ratio of the mesogenic core (the ratio of the length to diameter of the rod-like mesogens) on the side-chains, we designed the side-chain structure to be “phenyl–ester–phenyl” type. The synthetic routes to the monomers M3-5 and M2-5 are shown in Scheme 1, where M denotes monomer, numbers of 3 and 2 refer to the number of benzene rings in the side chain, and number of 5 is the number of carbon atoms of the tail. Both the monomers were synthesized by esterification of the substituted benzoic acid with the corresponding substituted phenol, whose chemical structures were confirmed by ^1H NMR, ^{13}C NMR, mass spectroscopy and elemental analysis (see the Experimental Section for details). M3-5 and M2-5 are white crystals at low temperatures. Upon heating from 20 to 160°C , only single melting process of crystals could be detected for M3-5 and M2-5, with the melting temperature of 141 and 81°C , respectively. The monomers can be readily dissolved in common organic solvents such as CHCl_3 , THF, and toluene. The resultant solutions are transparent and colorless.

To polymerize the monomers under mild conditions, we choose organorhodium complexes as the catalyst, which are robust with high tolerance to polar moiety in acetylene monomer and polar solvent (even in water³⁴ or air³⁵). In the Rh catalysts family, the zwitterionic Rh complex of $\text{Rh}(\text{nbd})[\text{B}(\text{C}_6\text{H}_5)_4]$ shows excellent activity even without any cocatalyst.^{36,37} For this reason, we chose it as the catalyst to carry out the polymerization in toluene.

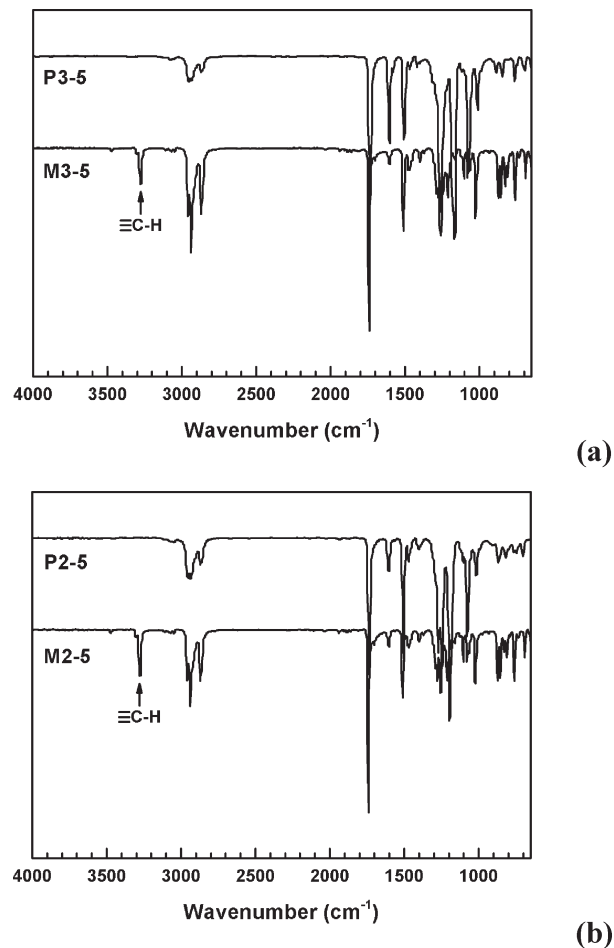


Figure 1. FT-IR spectra of the monomers and the corresponding polymers. (a) M3-5 and P3-5; (b) M2-5 and P2-5.

During the polymerization, both the colorless solutions of M3-5 and M2-5 turned to bright red and then became more and more turbid with lengthening reaction time, implying that the resultant polymers P3-5 and P2-5 formed aggregates. The red aggregates could not dissolve in common organic solvents such as *n*-octane, cyclohexane, toluene, CHCl_3 , THF, and DMF.

Since the polymer aggregates could not be dissolved in common organic solvents, the molecular characterization became somewhat difficult. Because of the poor solubility, we could not get the molecular weight (MW) information by such routine methods as GPC and laser light scattering, while the matrix-assisted laser desorption/ionization and time-of-flight mass spectroscopy (MALDI-TOF) method did not work either. However, as shown in Figure 1, the FT-IR results are still adequate to support that the polymerizations indeed give the desired polymers (or at least the oligomers). In the spectra of monomers, the $\equiv\text{C}-\text{H}$ vibration peaks at about 3300 cm^{-1} is clearly observed. Disappearance of this peak in the spectra of the polymerization products indicates that the alkynyl group $\text{C}\equiv\text{CH}$ has been consumed. We checked the thermal stability of the polymers. The TGA results (Figure 2) show that the temperatures for 5% weight loss of the samples are around 340°C in nitrogen atmosphere. The thermal stability of the polymers is considerably improved in comparison with PPA which degrades at about 270°C .³⁸ This implies that the backbones are protected by the large side-chains, which prevented the polymer from decomposing at low temperatures.³⁹

We used Raman technique to study the stereostructure of the polymer backbones. The Raman spectra reveal that both of P3-5

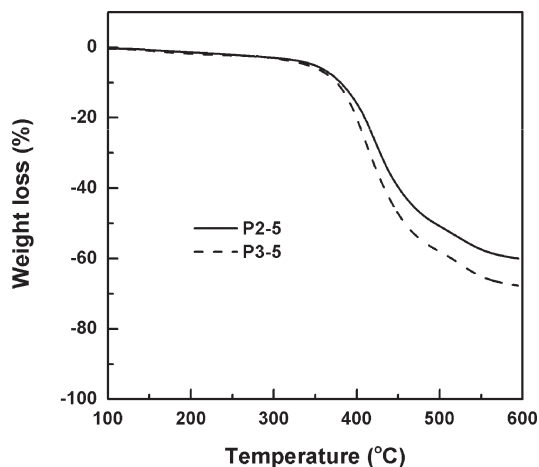


Figure 2. TGA results of P3-5 and P2-5 measured under nitrogen atmosphere.

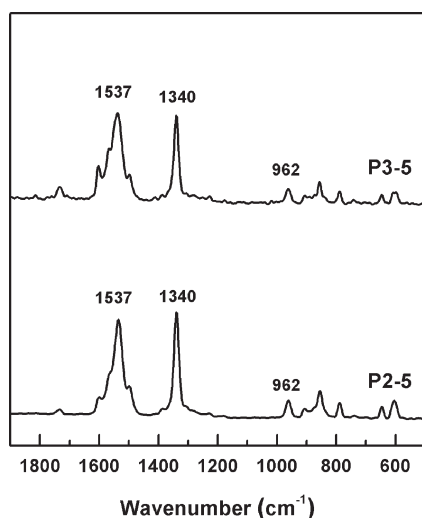


Figure 3. Raman spectra recorded from the red precipitates of P3-5 and P2-5.

and P2-5 possess *cis*-polyene structure (Figure 3). The peaks at 1537, 1340 and 962 cm^{-1} can be assigned to the stretching C=C band in *cis*-polyacetylene (although it is partially overlapped with that of the phenyl ring), the stretching vibration of *cis* C–C bond coupled with the single bond connecting the main chain and phenyl ring, and the C–H deformation band of the *cis* main-chain, respectively.^{40–42} On the other hand, the scattering peaks corresponding to the *trans* form, which shall appear at around 1480 and 1190 cm^{-1} ,^{42,43} are scarcely observed. Therefore, we conclude the red precipitates are *cis*-rich polyacetylenes. This result is consistent with that usually found in the monosubstituted polyacetylenes obtained from Rh-catalyzed polymerization, of which the main-chain is stereoregularly *cis*-transoidal.^{30,35}

We speculate that the insolubility of the polymers is related to the internal ordered structure of the precipitates, which can be detected by WAXD method. To prepare the WAXD samples, the insoluble precipitates were carefully washed with toluene to remove the residual monomers and catalysts. Therefore, the diffractions of the samples at room temperature shall solely be given by the polymer particles which were not subjected to any further thermal treatment. As depicted in Figure 4, the WAXD patterns of P3-5 and P2-5 clearly feature a smectic (or sanidic) structure. The diffractions up to the third-order with the scattering

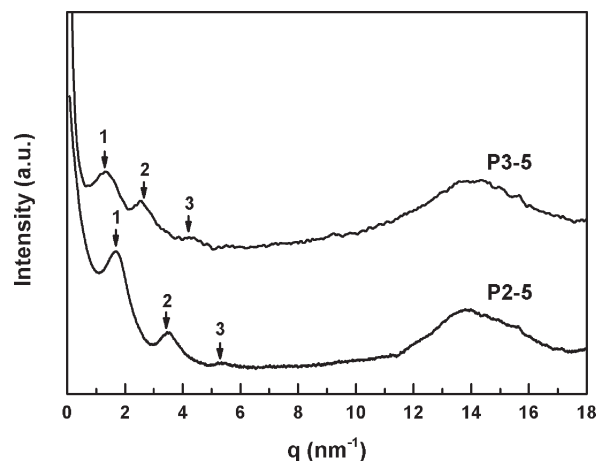


Figure 4. WAXD powder patterns of P3-5 and P2-5 solid particles obtained directly from solution polymerization.

vector ($q = 4\pi(\sin \theta)/\lambda$) ratio of 1:2:3 can be identified in the low-angle region, while in the high-angle region only an amorphous halo centered at a q value of $\sim 14 \text{ nm}^{-1}$ is observed. This result indicates that the smectic structure is developed within the solid particles right after they precipitated out from the polymerization solution. Compared to P2-5 with a shorter side-chain, P3-5 gives the diffractions appearing at lower angles, indicating that the smectic layer periodicity is side-chain length dependent. Our DSC experiments could not detect any first-order transition or glass transition of P3-5 and P2-5 from room temperature to 250 °C, implying that the polymers should be rigid and their LC transition temperatures could be higher than 250 °C (Since the *cis*-rich samples may degrade upon thermo treatment, we did not heat the samples to higher temperatures).

In our previous studies,^{22,23} we have identified that the molecule of poly(5-[(4'-alkoxy-4-biphenyl)carbonyl]oxy)-1-pentyne) with a relatively short spacer of three methylene units is sheet-like, which can stack parallel together to form a highly ordered smectic phase or monolayer lamellae in dilute solutions. For P3-5 and P2-5 without spacer, we consider that the LC structures observed shall be also constructed by the packing of whole sheet-like molecules, and the smectic (or sanidic) layer periodicity is determined by the width of the molecular sheet. It has been suggested that the *cis*-PPA derivatives without spacers can have the side-chains attached to the *cis*-transoidal backbone with a “herringbone” configuration for both head-to-tail and head-to-head arrangements.²⁴ Taking P3-5 as an example, Figure 5 depicts our molecular simulation result after energy minimization, which indeed shows a sheet-like conformation. Considering the angle of 60° between the polyacetylene backbone and the side-chain (see the top view in Figure 5), the width of the molecular sheet (L) should be $2l/\sin 60^\circ$, where l is the side-chain length with the alkyl tails in a fully extended conformation. As shown in Table 1, the d -spacings of the first-order diffractions (d_1 's) of P3-5 and P2-5 are almost identical to the calculated values of L . Considering that the mesogenic side-chains are tilted 30° away from the layer normal, one may assign the LC structure to be smectic C (S_C). Here, it is also worth mentioning that we in fact can take the whole sheet-like molecules as the building block of the LC structure. Therefore, we consider that the LC structure can belong to a sanidic structure with a one-dimensional long-range order along the layer normal (i.e., Σ_O phase suggested by Wendorff et al.).¹⁸

Figure 6 schematically depicts the molecular sheet and its smectic (or sanidic) packing of P3-5 and P2-5. Owing to the terminal attachment of the mesogens without flexible spacers, the side-chains and backbone are tightly coupled together. Therefore, the

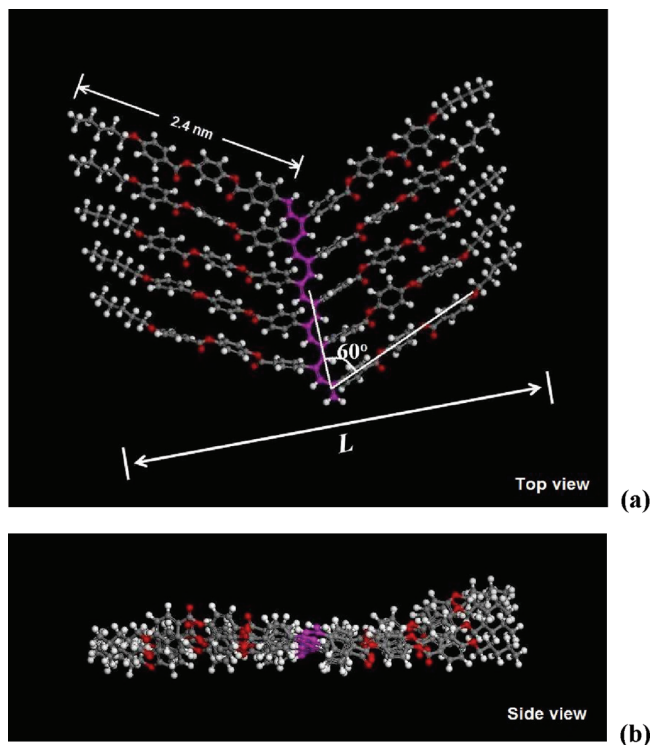


Figure 5. Illustrations of the sheet-like molecule of P3-5 after energy minimization: (a) top view; (b) side view. The carbon atoms on main chain are shown by pink color.

Table 1. Relationship between the Smectic Periodicity and the Molecular Width

polymer	q_1^a/nm^{-1}	d_1^a/nm	L^b/nm	d_1/L	LC structure
P3-5	1.48	4.24	4.15	1.02	S_C (or Σ_O)
P2-5	1.82	3.45	3.10	1.11	S_C (or Σ_O)

^aThe scattering vector (q_1) and the corresponding d -spacing (d_1) of the first-order diffraction. ^bMolecular width L obtained by molecular simulation with an assumption of all *trans* conformation for the methylene units.

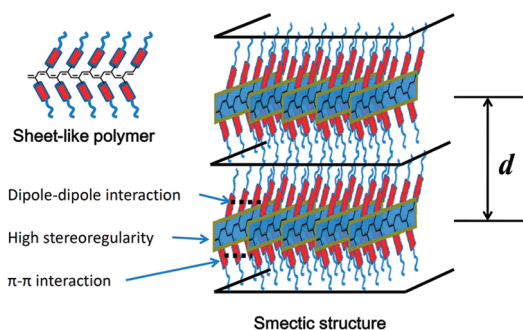


Figure 6. Schematic illustration of the smectic (or sanidic) structure of P3-5 and P2-5. Within each smectic layer, the polymer molecules are sheet-like and stack parallel to each other with the backbones located at the layer center.

molecule bears a rather rigid inner part including the planar *cis*-backbone and mesogenic cores on both sides of the backbone. In each smectic layer of the molecular stacking, the conjugated backbones are located at the center portion. We presume that the intermolecular interaction (including π - π stacking, dipole-dipole interaction, etc.) is so strong that the smectic aggregates of P3-5 and P2-5 cannot be dissolved in common organic solvents.

The morphology of the polymer particles directly precipitated out from the solutions was examined using SEM. The SEM

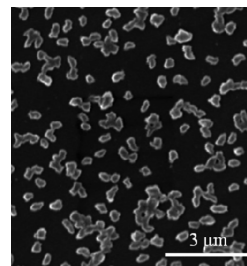


Figure 7. SEM image of the P3-5 solid particles obtained after the polymerization completed.

samples were prepared after the polymerization in toluene solution had completed. Because the trace residue monomers and catalysts can be neglected, the morphology observed should mainly come from the polymers. Figure 7 shows a SEM image of P3-5 particles. In some areas the larger aggregates are obviously the clusters of the small particles which adhered to each other. The isolated particles look relatively uniform,²⁹ with an average lateral size of ~ 300 nm. The polygonal and/or near rectangular shapes shall be largely associated with the smectic structure. For the rectangular shaped particles, the aspect ratio of the length to width can reach a value of ~ 3 . However, since the aggregation occurred during polymerization, the polymeric molecules were hard to adjust their packing in the solid particles. Therefore, the smectic structure is less perfect. On the basis of the WAXD profiles of P3-5 and P2-5 (Figure 4), the apparent correlation length along the smectic layer normal was estimated to be ~ 15 nm using the Scherrer equation, which is much smaller than the particle size observed under SEM.

We were interested in knowing when and how the smectic aggregates of P3-5 and P2-5 were formed in solution. It is reasonable to assume that the aggregation mechanism is very similar to that of crystallization during solution polymerization of crystalline polymers.⁴⁴ One may imagine that at the beginning of polymerization the resultant oligomers with relatively good solubility are dissolved in solution, so at that time the solution is transparent macroscopically. Once the oligomers further grow to a “critical MW”, the aggregation occurs. Afterward, the newly formed polymer (or oligomer) molecules may either assemble by themselves to form new aggregates, or join the existing solid particle leading to the particle growth in size. According to the morphology images showing that the polymer particles with large and relatively uniform size (see Figure 6), the latter case should be more possible. It is worth mentioning that the polymerization of M3-5 and M2-5 in toluene catalyzed by $\text{Rh}(\text{nbd})[\text{B}(\text{C}_6\text{H}_5)_4]$ proceeded considerably slowly at room temperature. Therefore, we could follow the polymerization process using various techniques, and thus the relationship between polymerization and aggregation can be studied in great detail.

Using UV-vis technique, we traced the polymerization process of M3-5 in toluene with a low initial monomer concentration ($[\text{M}]_0 = 0.23$ mmol/L) and a molar ratio of monomer/ $\text{Rh}(\text{nbd})[\text{B}(\text{C}_6\text{H}_5)_4]$ of 25:1. In the spectra shown in Figure 8a, the absorption band in the range from 400 to 550 nm is attributed to π - π^* electronic transition of the polyene backbone. This band appears rapidly and becomes a pronounced peak as the polymerization proceeds, whose position shifts to longer wavelength. The plot of the peak position of polyene backbone absorption vs polymerization time (t) illustrates that the red shift takes place very fast in the first 25 min and then gradually leaves off at ~ 455 nm after 60 min (Figure 8b). The bathochromic shift by ca. 25 nm of the peak position indicates a significant increase of the average conjugation length of P3-5, which may also partially reflect the increase of average MW. Note that it is seldom to obtain a *cis*-rich PPA with the main-chain absorption at such a long wavelength.

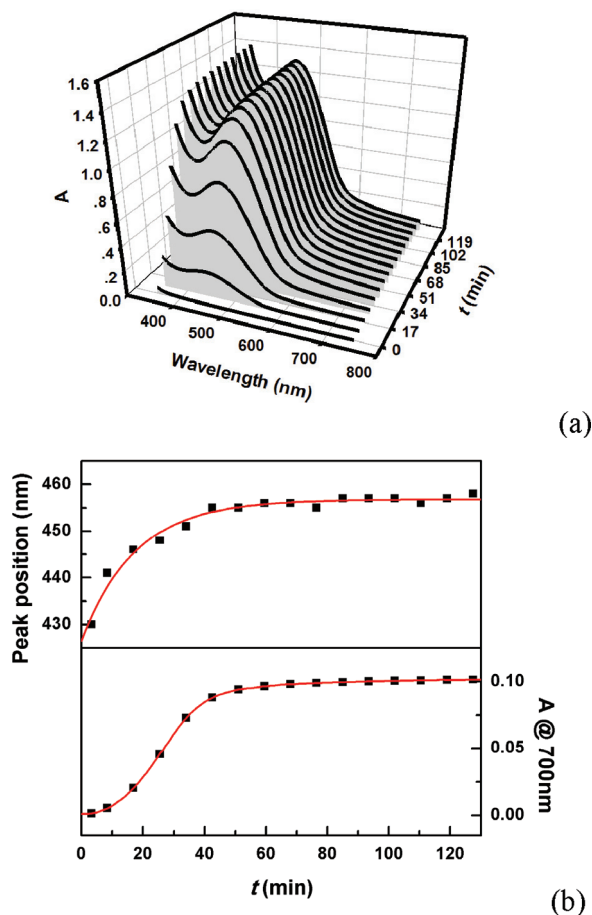


Figure 8. (a) In situ UV–vis detection of P3-5 polymerization at an initial monomer concentration ($[M]_0$) of 0.1 mg/mL. (b) Peak position of main-chain absorption and the value of “absorption” at 700 nm as a function of reaction time t . The absorption data were recorded continuously and repeatedly from 750 to 350 nm.

We consider that the rigid sheet-like shape of the P3-5 (also P2-5) molecules shall be rather persistent in solution and therefore, increasing MW will lead to the increase of conjugation length. Moreover, parallel packing of the molecules in the smectic structure may make the molecules more sheet-like.

In Figure 8a, we also observe the increase of “absorption” at 700 nm. As this wavelength is far away from the peak position of polyene backbone absorption at ~ 455 nm, we consider that the “absorption increment” at 700 nm should mainly arise from the scattering of the P3-5 particles formed during polymerization, which can thus be taken as a measurement of the solution turbidity. The value of “absorption” at 700 nm changing with t is also shown in Figure 8b, wherein a sigmoidal curve is observed with its largest slope located at t of ~ 25 min. The comparison between the two curves in Figure 8b reveals that at the beginning the overall aggregation of P3-5 molecules lags behind the increase of P3-5 conjugation length. This result infers that there is a “critical MW” for P3-5 aggregation.

To confirm the existence of the “critical MW”, we used PPh_3 as a terminator to stop the polymerization at various stages,³⁶ and tried to detect the trace amount of the residual soluble polymer (oligomer) in the solution via GPC. Taking M3-5 as an example, the polymerization was carried out in toluene with a $[M]_0$ of 10 mg/mL and a molar ratio of monomer/Rh(nbd)[$\text{B}(\text{C}_6\text{H}_5)_4$] of 25:1. At different t of polymerization, we transferred 0.2 mL of solution into a vial containing 5 mg of PPh_3 by filtration. After toluene in the vial was removed, the residual material was redissolved in THF for the GPC measurement. Figure 9 shows

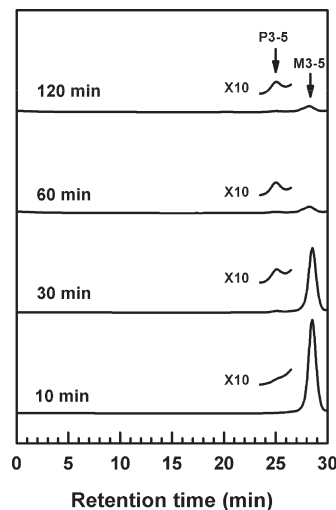


Figure 9. GPC curves of the soluble components obtained during the polymerization of M3-5 in toluene at different polymerization time. The $[M]_0$ was 10 mg/mL and the molar ratio of monomer/Rh(nbd)[$\text{B}(\text{C}_6\text{H}_5)_4$] was 25:1.

a set of GPC curves of the soluble compounds obtained at various t 's. The peak with a retention time of ca. 28.5 min corresponds to the monomer, this peak becomes smaller with increasing t . Interestingly, after 10 min of polymerization, a minor peak located at a retention time of ca. 25 min can be observed, which shall be related to the soluble P3-5 with an apparent number-average MW (M_n) of 2900 g/mol. This peak remains at the same position disregarding increasing t , indicating that the P3-5 with M_n over 2900 g/mol would precipitate out. Comparison between the apparent M_n 's of the two GPC peaks gives that the degree of polymerization of the soluble P3-5 is approximately 5. However, we are not able to determine the exact “critical MW” at this moment.

We monitored the whole polymerization process with different $[M]_0$'s using turbidity measurement. As mentioned above, we used the value of “absorption” at 700 nm as the solution turbidity. Figure 10a describes the changes in solution turbidity during the M3-5 polymerizations with a fixed monomer/Rh(nbd)[$\text{B}(\text{C}_6\text{H}_5)_4$] ratio of 25:1 and four $[M]_0$'s. Obviously, after an induction period the solution turbidity increases rapidly and then gradually levels off. An increase in $[M]_0$ leads to a shorter induction period and a steeper turbidity increase, which can be ascribed to the faster polymerization rate and more polymer molecules produced in solution. For polymerization of M2-5, a similar behavior of the turbidity change with t was observed. However, the aggregation ability of P2-5 is lower than that of P3-5. Figure 10b shows the comparison of turbidities as functions of t between M3-5 and M2-5, with a same $[M]_0$ of 2.3 mmol/L (i.e., 1 mg/mL for M3-5) and a monomer/Rh(nbd)[$\text{B}(\text{C}_6\text{H}_5)_4$] ratio of 25:1. It is found that shortening the length of mesogenic core can delay and damp the turbidity increase. We suggest that when more phenyl rings are incorporated into the molecules, the interaction (particularly π – π interactions between the side-chains) will be enhanced, resulting in a stronger tendency of aggregation of the sheet-like molecules in solutions.

We also monitored the polymerization using ^1H NMR technique to further investigate the relationship between polymerization and aggregation. Figure 11a shows a set of ^1H NMR spectra of M3-5 polymerization in toluene- d_8 recorded at 25 $^\circ\text{C}$ with an $[M]_0$ of 23 mmol/L (10 mg/mL) and a monomer/Rh(nbd)[$\text{B}(\text{C}_6\text{H}_5)_4$] molar ratio of 25:1. The resonance signal at δ 2.78 is assigned to the alkyne hydrogen ($\equiv\text{CH}$) of the monomer,

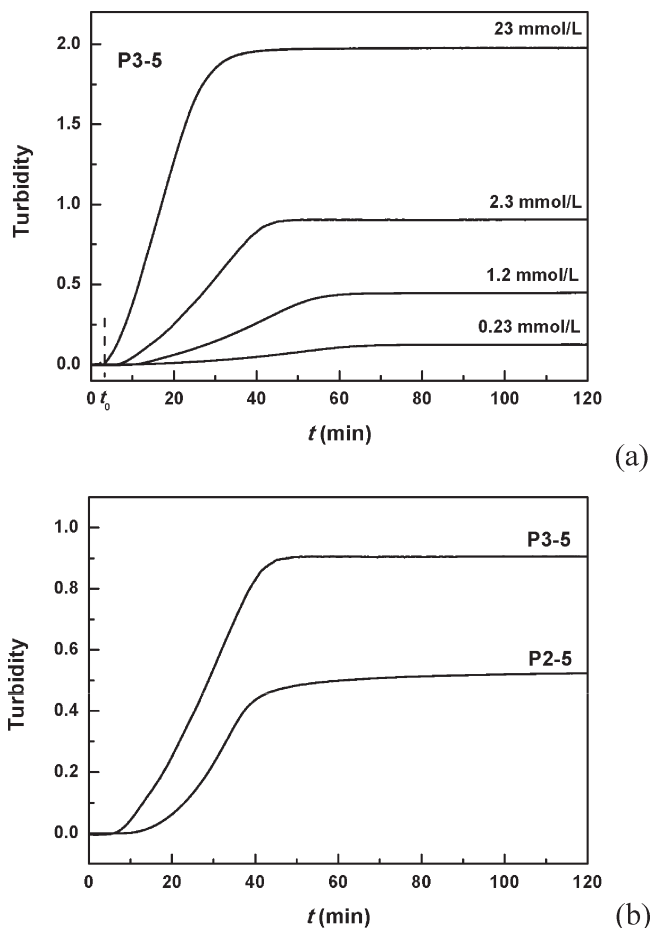


Figure 10. (a) In situ turbidity detection of the P3-5 polymerization with different initial monomer concentrations ($[M]_0$'s) at a wavelength of 700 nm. (b) Turbidities as functions of t for P3-5 and P2-5 at a fixed $[M]_0$ of 2.3 mmol/L.

while that centered at δ 3.55 is attributed to the hydrogen of $-\text{OCH}_2$ group on the side-chains. At the beginning of polymerization (e.g., at $t = 4$ min), the originally well-resolved peaks of $-\text{OCH}_2$ becomes obviously broad. This may be attributed to that the signal of the $-\text{OCH}_2$ groups in the soluble polymer molecules with reduced mobility is superimposed on that of the monomers. When the monomer concentration is continuously decreased with increasing t , the signal of $-\text{OCH}_2$ turns to be an apparently single broad one. We expect that the environment of $-\text{OCH}_2$ shall be very rigid when the P3-5 molecules are packed into the aggregates, and the corresponding signal will be hardly detected. However, $-\text{OCH}_2$ signal can be found in a fairly long time of polymerization (up to 60 min), reflecting that the newly formed P3-5 with low MW is dissolved in the solution. This observation suggests again that only when the P3-5 molecules reach a "critical MW" or the solubility limit, they will pack into the aggregates with smectic structure.

The concentration of the monomer $[M]$ is proportional to the integration of alkyne hydrogen ($\equiv\text{CH}$) resonance peak at δ 2.78, and therefore, the value of $[M]/[M]_0$ is equal to the ratio of the integrated area at a reaction time of t to that recorded at $t = 0$. In Figure 11b, we plot the monomer conversion of $\{1 - [M]/[M]_0\}$ measured from the ^1H NMR spectra as a function of t . Apparently, there are two stages of polymerization. The first stage is ranged from t of ~ 3 to ~ 30 min. It is observed that after a short induction time of ~ 3 min, the monomer conversion increases rapidly with increasing t , seemingly showing a linear behavior. At $t > \sim 30$ min (the second stage of polymerization), the overall

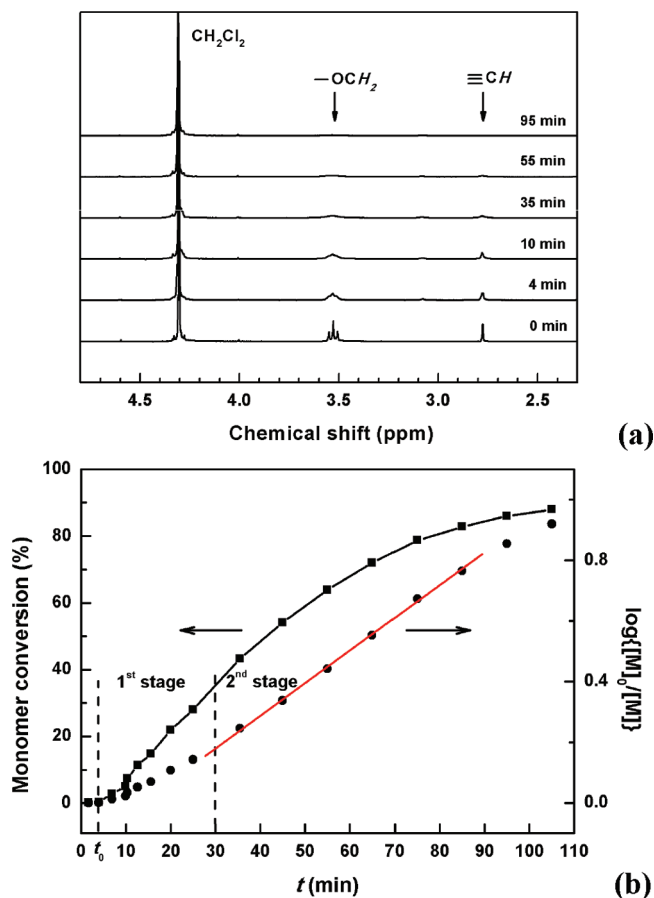
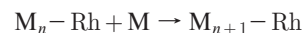


Figure 11. In-situ ^1H NMR monitoring of P3-5 polymerization with DCM as the internal standard in toluene- d_8 . The initial monomer concentrations ($[M]_0$) is 10 mg/mL. (a) Set of ^1H NMR spectra recorded at various t 's. (b) Monomer conversion $\{1 - [M]/[M]_0\}$ and $\log\{[M]/[M]_0\}$ as functions of t . The value of $[M]/[M]_0$ was measured from the ^1H NMR spectra.

polymerization rate, i.e., the slope of the conversion curve becomes smaller than that of the first stage. Note that the reaction condition applied for the ^1H MNR measurement is identical to that for the turbidity measurement with $[M]_0 = 23$ mmol/L (10 mg/mL) (see Figure 10a). We find that the induction time of polymerization is rather close to the onset of turbidity increase indexed as t_0 in Figure 10a. Moreover, while the polymerization enters the second stage, the turbidity in fact approaches the plateau value. Although the turbidity and ^1H NMR result were measured from different experiments and thus the comparison between them cannot be made strictly, the coincidences still indicates that the aggregation indeed occurs at the early stage of polymerization, and is closely related to the polymerization process. Since the onset of turbidity increase locates at the very beginning of polymerization, we suspect that once the polymerization takes place, the P3-5 molecules possess a MW distribution, of which the largest ones form aggregates immediately. On the other hand, we note that at t of ~ 90 min the residual resonance of the alkyne hydrogen is still detectable, implying that the monomers are not fully exhausted. Therefore, during a long period of time, the aggregation and polymerization occur simultaneously.

According to the literatures,^{30,45} an insertion mechanism is generally accepted for the Rh-catalyzed acetylene polymerization. Thus, a simple propagation reaction can be described as:



where $M_n - \text{Rh}$ and M denote the intermediate active propagation chain and the monomer, respectively. Therefore, the propagation

rate can be written as $-d[M]/dt = k[M][M_n-Rh]$, where k is the rate constant. The above rate formula can be rewritten as $\log\{[M]_0/[M]\} = k[M_n-Rh]t$. Interestingly, we find that the plot of $\log\{[M]_0/[M]\} \sim t$ presents a linear behavior for the second stage of polymerization (i.e., $t > 30$ min), inferring that the concentration of active propagation chain $[M_n-Rh]$ is nearly constant. On the other hand, we observe that the slope of $\log\{[M]_0/[M]\} \sim t$ curve for the first stage of polymerization is always smaller. Assuming that the value of k remains constant during the whole polymerization process, the smaller slope indicates that the $[M_n-Rh]$ is lower. In addition to the possibly unstable initiation process of M3-5 polymerization with the catalyst of $Rh(nbd)[B(C_6H_5)_4]$, we presume that the rather fast aggregation occurred in the first stage of polymerization greatly affects the value of $[M_n-Rh]$. The Rh complex at the chain ends might either be trapped in the solid particles after the chain packing or be released to solution later on; however, we cannot determine which one of the two possibilities is more likely on the basis of the polymerization kinetics data we obtained.

After both the processes of aggregation and polymerization slow down, namely, after the first stage, the polymerization seems to enter a steady state, giving the apparent first-order polymerization kinetics, whose behavior is highly reminiscent of that observed in traditional acetylene polymerization under catalyst system of $Ti(OBu)_4-AlEt_3$.⁴⁶ For the $Ti(OBu)_4-AlEt_3$ catalyzed acetylene polymerization, the propagation mechanism is believed to be *cis*-insertion of monomer, wherein the active site remaining relatively constant is attributed to the presence of two types of active sites. Although we are unable to deduce a similar explanation for our polymerization system, we still consider that the first-order polymerization process we observed deserves further investigation, which may be utilized to control the growth of polymer products. Furthermore, when the resultant polymers can form uniform nanoparticles directly during polymerization,²⁹ we might take advantage of the first-order polymerization to develop a technique to control the particle morphology.

For P3-5 and P2-5 molecules which can aggregate during solution polymerization, we consider that the rigid sheet-like molecular structure with the mesogenic side chain directly linked to the polyacetylene backbone plays an important role. However, according to the literatures, such arrangement of backbone and mesogenic side-chain may not be certain to result in the spontaneous molecular assembly in solutions. Advincula et al. synthesized a monomer of 4-(dodecyloxy)phenyl 4-ethynylbenzoate (denoted as M2-12 below). Compared to M2-5, M2-12 just possesses a longer alkyl tail with 12 carbon atoms.²⁵ After polymerizing M2-12 under WCl_6 in dry toluene, they have found that the resultant polymer (denoted as P2-12) possesses a very good solubility in common organic solvent. In our work, we also synthesized P2-12 using $Rh(nbd)[B(C_6H_5)_4]$ as the catalyst, with an attempt to improve the solubility of the polymer with increasing the side-chain tail length. In contrast to that obtained by Advincula et al., we found that the polymerization behavior of M2-12 was similar to that of M2-5, and the red P2-12 was insoluble. It seems that the detailed chain stereostructures affect the polymer solubility. It is known that polymerization of acetylene monomer with W-based catalyst usually yields *trans*-rich main chain, while the catalyst of rhodium complexes usually gives *cis*-rich structure. However, considering that a perfect *trans*-cisoidal main chain is actually rather planar, we suspect that the polymer backbone of the sample synthesized by Advincula et al. might be stereorandom with a relatively lower *trans*-content, namely, have more conformational defects.

In addition to the stereoregularity effect of the backbone, the $\pi-\pi$ interaction of the phenyl ring and the dipole-dipole interaction of the ester linkage in the mesogenic side chain may also play important roles in the solution aggregation of the

polymers we studied. Hsu et al. have synthesized a monomer of 4-ethynylphenyl 4-pentylcyclohexanecarboxylate and polymerized it by $[Rh(nbd)Cl]_2$.²⁷ The resultant polymer has good solubility but exhibits no LC structure. In comparison with P2-5, it seems that introducing a cyclohexyl ring, which may display either chair or boat conformation, to the side-chain weakens the interaction between side-chains and thus disfavor the LC ordering. Tang et al. have reported that polymerization of 2-(4-octoxyphenyl)-5-(4-ethynylphenyl)-1,3,4-oxadiazole using $[Rh(nbd)Cl]_2$ as the catalyst also gives a soluble polymer in common organic solutions.⁴⁷ Compared with M2-5, their monomer changes the ester linkage in the side chain to the 1,3,4-oxadiazole moiety which can also provide significant $\pi-\pi$ interaction. At this stage, it is hard for us to conclude what chemical structure of side-chain polyacetylene with mesogenic group directly attached to the backbone will lead to sheet-like molecules which can undergo solution LC ordering spontaneously. Therefore, in order to increase the effective conjugation length of the sheet-like polyacetylene and to obtain better LC ordering, a more systematic study is required.

Summary

We have successfully synthesized two side-chain liquid-crystalline polyacetylenes (P3-5 and P2-5) with the mesogenic unit directly linked to the semirigid backbone in a terminal-on mode. Our experimental results show that during the polymerization reactions, both P3-5 and P2-5 can directly self-aggregate into red insoluble nanoparticles with fairly uniform size of ~ 300 nm. The *cis*-rich P3-5 and P2-5 are sheet-like. After reaching a "critical MW" during polymerization, they may stack parallel to each other with strong intermolecular interaction, forming smectic or sanidic structure. P3-5 with larger slenderness ratio of the mesogenic unit has stronger aggregation capability than P2-5. During the polymerization process, the fast aggregation is well correlated to the fast polymerization. Afterward, the polymerization reaches a steady state with a first-order kinetics. It is worth noting that the effective conjugation length of the *cis*-rich P3-5 and P2-5 we obtained is considerably long. Therefore, the molecular design described in this paper may provide a method to directly produce high performance opto-electronic materials of polyacetylene derivatives with improved properties.

Acknowledgment. This work was supported by the National Natural Science Foundation of China (NNSFC Grants: 20129001, 20874082, 20774006, 20990232 and 20974028) and the Research Grants Council of Hong Kong (602707).

References and Notes

- (1) Akagi, K. *J. Polym. Sci., Part A: Polym. Chem.* **2009**, *47*, 2463–2485.
- (2) Liu, J.; Lam, J. W. Y.; Tang, B. Z. *Chem. Rev.* **2009**, *109*, 5799–5867.
- (3) Lam, J. W. Y.; Tang, B. Z. *J. Polym. Sci., Part A: Polym. Chem.* **2003**, *41*, 2607–2629.
- (4) Choi, S. K.; Gal, Y. S.; Jin, S. H.; Kim, H. K. *Chem. Rev.* **2000**, *100*, 1645–1681.
- (5) Liu, K.-P.; Yu, Z.-Q.; Liu, J.-H.; Chen, E.-Q. *Macromol. Chem. Phys.* **2009**, *210*, 707–716.
- (6) Lam, J. W. Y.; Tang, B. Z. *Acc. Chem. Res.* **2005**, *38*, 745–754.
- (7) Finkelmann, H.; Happ, M.; Portugall, M.; Ringsdorf, H. *Makromol. Chem.* **1978**, *179*, 2541–2544.
- (8) Moigne, J. L.; Hilberer, A.; Kajzar, F. *Makromol. Chem.* **1992**, *193*, 515–530.
- (9) Oh, S.-Y.; Ezaki, R.; Akagi, K.; Shirakawa, H. *J. Polym. Sci., Part A: Polym. Chem.* **1993**, *31*, 2977–2985.
- (10) Oh, S.-Y.; Akagi, K.; Shirakawa, H.; Araya, K. *Macromolecules* **1993**, *26*, 6203–6206.
- (11) Vicentini, F.; Mauzac, M.; Laversonne, R.; Pochat, P.; Parneix, J. P. *Liq. Cryst.* **1994**, *16*, 721–733.

- (12) Akagi, K.; Shirakawa, H. *Macromol. Symp.* **1996**, *104*, 137–158.
- (13) Koltzenburg, S.; Wolff, D.; Stelzer, F.; Springer, J.; Nuyken, O. *Macromolecules* **1998**, *31*, 9166–9173.
- (14) Kong, X. X.; Tang, B. Z. *Chem. Mater.* **1998**, *10*, 3352–3363.
- (15) Lam, J. W. Y.; Kong, X. X.; Dong, Y. P.; Cheuk, K. K. L.; Xu, K. T.; Tang, B. Z. *Macromolecules* **2000**, *33*, 5027–5040.
- (16) Tang, B. Z.; Kong, X. X.; Wan, X. H.; Peng, H.; Lam, W. Y.; Feng, X. D.; Kwok, H. S. *Macromolecules* **1998**, *31*, 2419–2432.
- (17) Demus, D.; Goodby, J. W.; Gray, G. W.; Spiess, H.-W.; Vill, V. *Physical Properties of Liquid Crystals*; Wiley-VCH: Weinheim, Germany, 1999.
- (18) Ebert, M.; Herrmann-Schonherr, O.; Wendorff, J. H.; Ringsdorf, H.; Tschirner, P. *Liq. Cryst.* **1990**, *7*, 63–79.
- (19) Stagnaro, P.; Cavazza, B.; Trefiletti, V.; Costa, G.; Gallot, B.; Valenti, B. *Macromol. Chem. Phys.* **2001**, *202*, 2065–2073.
- (20) Stagnaro, P.; Conzatti, L.; Costa, G.; Gallot, B.; Tavani, C.; Valenti, B. *Macromol. Chem. Phys.* **2003**, *204*, 714–724.
- (21) Stagnaro, P.; Conzatti, L.; Costa, G.; Gallot, B.; Valenti, B. *Polymer* **2003**, *44*, 4443–4454.
- (22) Ye, C.; Xu, G. Q.; Yu, Z. Q.; Lam, J. W. Y.; Jang, J. H.; Peng, H. L.; Tu, Y. F.; Liu, Z. F.; Jeong, K. U.; Cheng, S. Z. D.; Chen, E. Q.; Tang, B. Z. *J. Am. Chem. Soc.* **2005**, *127*, 7668–7669.
- (23) Yu, Z. Q.; Liu, J. H.; Yan, J. J.; Liu, X. B.; Liang, D. H.; Lam, J. W. Y.; Dong, Y. P.; Li, Z. C.; Chen, E. Q.; Tang, B. Z. *Macromolecules* **2007**, *40*, 8342–8348.
- (24) Moigne, J. L.; Hilberer, A.; Strazielle, C. *Macromolecules* **1992**, *25*, 6705–6710.
- (25) Advincula, R. C.; Duran, R. S.; Moigne, J. L.; Hilberer, A. *Macromolecules* **1993**, *26*, 3895–3903.
- (26) Teraguchi, M.; Masuda, T. *Macromolecules* **2000**, *33*, 240–242.
- (27) Ting, C. H.; Chen, J. T.; Hsu, C. S. *Macromolecules* **2002**, *35*, 1180–1189.
- (28) Ober, C. K. *Science* **2000**, *288*, 448–449.
- (29) Kimura, K.; Kohama, S.; Yamazaki, S. *Polym. J.* **2006**, *38*, 1005–1022.
- (30) Mayershofer, M. G.; Nuyken, O. *J. Polym. Sci., Part A: Polym. Chem.* **2005**, *43*, 5723–5747.
- (31) Melissaris, A. P.; Litt, M. H. *J. Org. Chem.* **1992**, *57*, 6998–6999.
- (32) Orzeszko, B.; Melon-Ksyta, D.; Orzeszko, A. *Synth. Commun.* **2002**, *32*, 3425–3429.
- (33) Schrock, R. R.; Osborn, J. A. *Inorg. Chem.* **1970**, *9*, 2339–2343.
- (34) Tang, B. Z.; Poon, W. H.; Leung, S. M.; Leung, W. H.; Peng, H. *Macromolecules* **1997**, *30*, 2209–2212.
- (35) Sedlacek, J.; Vohlidal, J. *Collect. Czech. Chem. Commun.* **2003**, *68*, 1745–1790.
- (36) Kishimoto, Y.; Itou, M.; Miyatake, T.; Ikariya, T.; Noyori, R. *Macromolecules* **1995**, *28*, 6662–6666.
- (37) Nakazato, A.; Saeed, I.; Katsumata, T.; Shiotsuki, M.; Masuda, T.; Zednik, J.; Vohlidal, J. *J. Polym. Sci., Part A: Polym. Chem.* **2005**, *43*, 4530–4536.
- (38) Masuda, T.; Tang, B. Z.; Higashimura, T.; Yamaoka, H. *Macromolecules* **1985**, *18*, 2369–2373.
- (39) Tang, B. Z.; Wan, X. H.; Kwok, H. S. *Eur. Polym. J.* **1998**, *34*, 341–345.
- (40) Lefrant, S.; Lichtmann, L. S.; Temkin, H.; Fitchen, D. B.; Miller, D. C.; Whitwell, G. E.; Burlitch, J. M. *Solid State Commun.* **1979**, *29*, 191–196.
- (41) Tabata, M.; Takamura, H.; Yokota, K.; Nozaki, Y.; Hoshina, T.; Minakawa, H.; Kodaira, K. *Macromolecules* **1994**, *27*, 6234–6236.
- (42) Tabata, M.; Tanaka, Y.; Sadahiro, Y.; Sone, T.; Yokota, K.; Miura, I. *Macromolecules* **1997**, *30*, 5200–5204.
- (43) Shirakawa, H.; Ito, T.; Ikeda, S. *Polym. J.* **1973**, *4*, 460–462.
- (44) Mucha, M.; Wunderlich, B. *J. Polym. Sci., Part B: Polym. Phys.* **1974**, *12*, 1993–2018.
- (45) Kishimoto, Y.; Eckerle, P.; Miyatake, T.; Kainosho, M.; Ono, A.; Ikariya, T.; Noyori, R. *J. Am. Chem. Soc.* **1999**, *121*, 12035–12044.
- (46) Chien, J. C. W. *Polyacetylene: Chemistry, Physics, and Material Science*; Academic Press: Orlando, FL, 1984.
- (47) Wang, X.; Wu, J. C.; Xu, H. Y.; Wang, P.; Tang, B. Z. *J. Polym. Sci., Part A: Polym. Chem.* **2008**, *46*, 2072–2083.